Progress In Electromagnetics Research C, Vol. 132, 79–88, 2023

Reconfigurable Frequency Selective Surfaces for X Band Applications

Anett Antony[1, *], Sayantani Dutta[1], Bidisha Dasgupta[1], and Anamiya Bhattacharya[2]

Abstract—The paper presents a new technique for designing a reconfigurable frequency selective surface (RFSS) by mechanical means. The combination of triangular loop element and three-legged element has been used to design the proposed single substrate two sided frequency selective surface (FSS) structure which offers variable transmission coefficient characteristics over the X-band frequencies under TE polarization for different angles of incidence. Thus, the band stop characteristics can be reconfigured by changing incident angle which describes the structure as 'reconfigurable reflector'. The proposed FSS geometry is polarization insensitive under both TE and TM polarizations. The simulated results are further cross verified by conducting measurement of the fabricated structure. The equivalent circuit model (ECM) of the proposed FSS geometry has been provided, and the equivalent circuit parameters of the proposed FSS geometry have also been extracted using the curve fitting techniques. The proposed FSS structure can be used as a frequency reconfigurable reflector surface/reconfigurable intelligent surface (RIS) for advanced wireless communication.

1. INTRODUCTION

Periodic structures are widely used over a very wide electromagnetic spectrum starting from microwave and millimetre-wave to THz and optical bands. Frequency selective surface (FSS) is a periodic structure arranged on a dielectric and has the frequency discrimination property to control the propagation of an electromagnetic (EM) wave, like transmission or reflection, depending on the characteristics of the periodic structure. The concept of FSS originates long time back, but the research on FSS has created a new era in the field of applied electromagnetics since last few decades for designing filter, reflector, polariser, absorber, etc. [1]. With the ever growing demand of wireless technology, multifunctional devices, the demand for reconfigurable/tunable FSS (RFSS) is increasing day by day for designing intelligent walls, tunable radomes, reflector for reconfigurable antennas and for adaptive screening of unwanted transmissions [2–5]. Mechanical tuning and insertion of discrete electronic components are two main approaches for designing RFSS [2–5]. The electronic tuning by the insertion of PIN/Varactor diodes, solid state or micro-electro-mechanical system (MEMS) switches is a common approach, but it involves design complexity and also requires additional suitable biasing network [6–8], whereas FSS can be mechanically tuned by employing mechanical modifications such as stretching, folding, shifting, or rotating FSS elements [2–5]. Abadi et al. presented techniques for designing large-scale, mechanically tunable periodic structures (PSs) by adopting three techniques, like overlapping combined with relative movement, stretching/compression, and flexure which ultimately tuned the capacitance and inductance of elementary periodic structures with capacitive and inductive surface impedances over wide ranges of values [2]. Ferreira et al. reported a mechanically tunable 3D FSS by rotating an inner element, and the structure was inspired by the classical square slot design [3]. Azemi et al. designed a 3-D spring FSS structure which can be tuned mechanically by altering the height of a spring-shaped unit-cell

Received 3 March 2023, Accepted 10 April 2023, Scheduled 16 April 2023

* Corresponding author: Anett Antony (anett.anthony@iiitg.ac.in).

[1] Department of Electronics and Communication Engineering, Indian Institute of Information Technology, Guwahati, India. [2] Space Applications Centre, Indian Space Research Organization, Microwave Remote Sensors Area, Ahmedabad, India.

resonator [4]. Silva et al. presented a work on reconfigurable FSS where the angular instability of the FSS was used in the development of reconfigurable structures through its rotation [5].

Some of the past research works on RFSS are summarized in Table 1 [2, 3, 5–10]. The proposed work presents a very simple technique for designing RFSS which provides frequency hopping/reconfigurability by changing the angle of incidence. No active element and additional biasing network are used in the proposed designing. A new type of single substrate two sided FSS geometry is presented which is realised by taking the combination of a loop type and a center connected type element. The proposed structure offers variable frequency band (stopband) over the X band under TE polarization. Further, the transmission line equivalent circuit model of the proposed geometry has been obtained from the frequency response characteristic, and the corresponding circuit parameters have been extracted using curve fitting techniques [11–14]. The development of the structure and its performance analysis have been carried out by using EM simulator CST [15]. The unit cell FSS geometry is presented under Section 2. Section 3 presents the chronological development of proposed FSS geometry and its equivalent transmission line circuit model. Section 4 presents the measured results. Finally, Section 5 concludes the paper.

Table 1. Comparison of the proposed FSS structure with some other existing works.

Ref., Year	Shape of FSS	Targeted Frequency band (in GHz)	Method adopted	Size of FSS unit cell (in mm)
2021, [6]	Rectangular strips	3.62–4.25	Varactor diode	$10 \times 10 \times 0.6$
2021, [7]	Square-slot	4.84–5.90	Varactor diode	$9 \times 9 \times 0.508$
2020, [8]	Rectangular loop like with plus shaped structure	3.5–5.7	Varactor diode	$6 \times 6 \times 0.12$
2020, [9]	Cross dumbbell shaped	3.2–5.5	rotating the horizontal grid orientation manually	$18 \times 18 \times 0.1$
2019, [10]	Jerusalem crosses on top and bottom layer comprises an aperture-based geometry	3.7–4.27	Varactor and pin diode	$10 \times 10 \times 1$
2017, [3]	Inspired by the classical flat square slot FSS	2.4–4	rotation of a movable inner element	$34.5 \times 34.5 \times 2$
2017, [5]	Triangular patches	Around 8–10	Changing the incident angle by rotating the structure	$20 \times 20 \times 1.5$
2016, [2]	Long Metallic strips	About 5–9	relative movement, stretching/compression, and flexure	Metallic strips of width 2 mm with gap of 3 mm
Proposed work	Both sides triangular loop with three-legged element	8–12	Changing the incident angle	$14 \times 14 \times 1.5$

2. THE FSS GEOMETRY

Different versions of FSS structures, realised using triangular loop type and center connected element type geometries are investigated, as shown in Figs. 1(a), (b), and (c), respectively. The substrate used here is an inexpensive, both side copper coated single layer of FR-4 material with dielectric constant $\varepsilon_r = 4.4$, height $(t_{sub}) = 1.5\,\text{mm}$, metal thickness $(t_{\text{FSS}}) = 0.035\,\text{mm}$, and dimension $l \times w$ along the X-axis and Y-axis, respectively. Structure 1 is made up of two triangular loops (TLs) in both the top and bottom sides of the substrate and is shown in Fig. 1(a). Structure 2 consists of a three-legged element loaded triangular loop (TL-3L) in the top side and a triangular loop (TL) in the bottom side as shown in Fig. 1(b). Structure 3 is made up of TL-3L in both the top and bottom sides of the substrate and is shown in Fig. 1(c). The dimensions of proposed geometry after parametric optimization are given in the caption of Fig. 1.

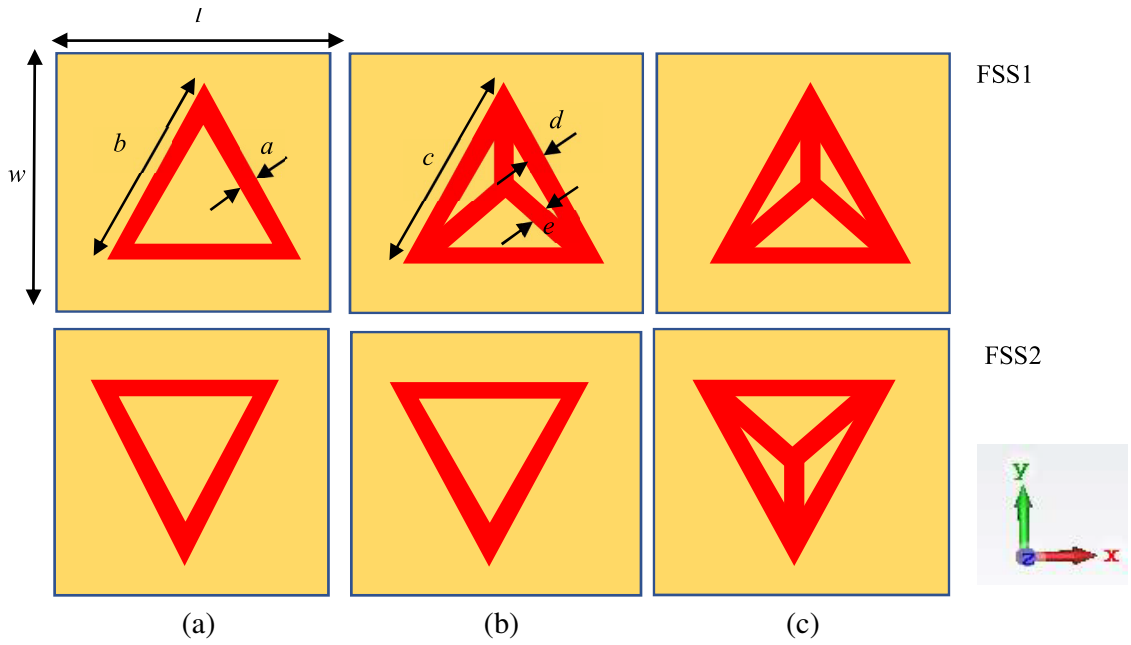

Figure 1. FSS structures: (a) structure 1 (triangular loop (TL) in top and TL in bottom layer), (b) structure 2 (three-legged loaded triangular loop (TL-3L) in top and TL in bottom layer), and (c) structure 3/proposed structure (TL-3L in top and bottom layer). (The dimension of the parameters (in mm) is given as $w = 14$, $l = 14$, $a = d = 1$, $b = 6.5$, $c = 6.5$, $e = 2$).

3. CHRONOLOGICAL DEVELOPMENT OF THE FSS STRUCTURE

A TL geometry has been initially selected to develop unit cell FSS geometry. Further, a 3L element has been introduced. In order to achieve wide stopband transmission characteristics, three different versions of two-layered FSS structures have been characterized which are reported in detail in the subsequent paragraphs. When an FSS behaves as a reflector, its reflection parameter S_{11} should be near 0 dB, and the transmission parameter S_{21} should be less than or equal to $-10\,\text{dB}$ over the required band [16].

Single layer FSS: The first step is to study the transmission coefficient characteristics of a unit cell element made up of a TL and 3L elements respectively on an FR4 dielectric substrate of height 1.5 mm of dimension $l \times w$. The simulated transmission characteristics offer a stopband from 9 GHz to 10.68 GHz for TL structure and 10.74 GHz to 11.3 GHz for 3L structure, as shown in Fig. 2(a). In the next stage, a 3L structure was introduced along with TL, improving the stopband which varies from 10.69 GHz to 12.5 GHz, as shown in Fig. 2(a). So, it is observed that TL-3L structure provides slightly better bandwidth than the TL structure, and also the bandwidth gets shifted to the higher side of the

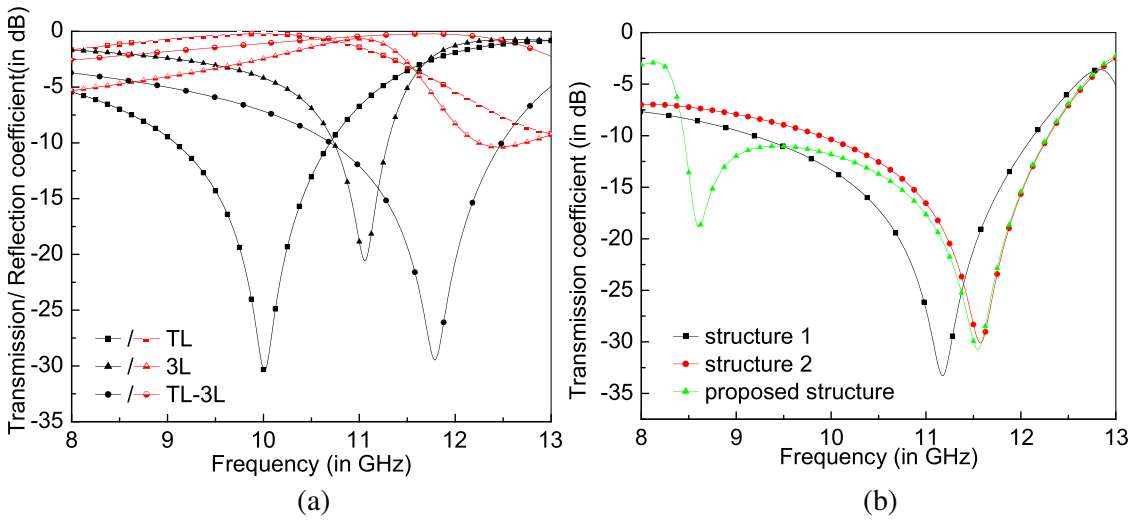

Figure 2. (a) Transmission coefficient (S_{21}) and reflection coefficient (S_{11}) characteristics for the isolated shapes: triangular loop (TL) structure, three legged (3L) structure and three legged with triangular shaped (TL-3L) structure for TE polarization and (b) transmission coefficient characteristics for structure 1, structure 2, and proposed FSS.

frequency spectrum than that of the TL structure. The reflection coefficient characteristics have also been shown along with the transmission coefficient characteristics in Fig. 2(a) to show the non-absorbing characteristics of the FSS structure.

Two layered FSS: In order to improve the bandwidth [17, 18] (i.e., $S_{21} \leq -10\,\text{dB}$), three combinations of the two layered FSS structure have been investigated, namely (a) structure 1: both sides TL, (b) structure 2: TL-3L and TL, and (c) proposed structure: both sides TL-3L. Although the single layer triangle-shaped FSS geometry is asymmetrical, in single substrate two layered FSS structure, both the TL-3Ls at the top and bottom sides are placed in such an orientation that their combination is like a 'Star' which is symmetrical. Structure 1 provides wide transmission bandwidth over 9.23–12.14 GHz as shown in Fig. 2(b). Structure 2 provides a wide transmission bandwidth over 9.89–12.29 GHz. The proposed FSS, which is structure 3, provides better bandwidth than the other two structures, i.e., 8.44 GHz to 12.28 GHz, so was chosen as the final proposed structure. The effect of rotation angles up to 45 degrees has been investigated for both TE and TM polarizations by varying the angle of incidence, i.e., theta (θ) in each structure. The frequency hopping characteristics over the X-band under TE polarization when the angle of incidence varies from 0° to 45° are shown in Figs. 3(a), (b), and (c) for structures 1, 2, and the proposed structure, respectively. However, the transmission coefficient characteristics for oblique incidence under TM polarization are almost the same as normal incidence for all the structures, and the characteristics for the proposed structure are shown in Fig. 3(d). For the proposed structure the lowest frequency point remains unchanged while the highest frequency point shifts towards the lower side of spectrum as the angle of incidence increases from 0° to 45°.

For the proposed geometry the reflection characteristics are near 0 dB (non-absorbing), and the reflection phases are approximately linear over the whole working band at different incidence angles, and the same is shown in Figs. 3(e) and (f), respectively. The polarization stability is checked by varying the angle phi (Φ). The proposed FSS geometry is polarization insensitive under both TE and TM polarizations, which can be due to the overall symmetricity of the proposed structure as shown in Fig. 4.

Equivalent Circuit Model (ECM): The ECM of the proposed FSS structure is shown in Fig. 5(a). The transmission coefficient (S_{21}) can be analysed using the relationship between the S parameters and $ABCD$ parameters of the cascaded circuit as given below [11].

$$\begin{bmatrix} A & B \\ C & D \end{bmatrix} = \begin{bmatrix} 1 & 0 \\ jY_{\text{FSS1}} & 1 \end{bmatrix} \cdot \begin{bmatrix} \cos\varphi & jZ_1 \sin\varphi \\ j\dfrac{\sin\varphi}{Z_1} & \cos\varphi \end{bmatrix} \cdot \begin{bmatrix} 1 & 0 \\ jY_{\text{FSS2}} & 1 \end{bmatrix} \tag{1}$$

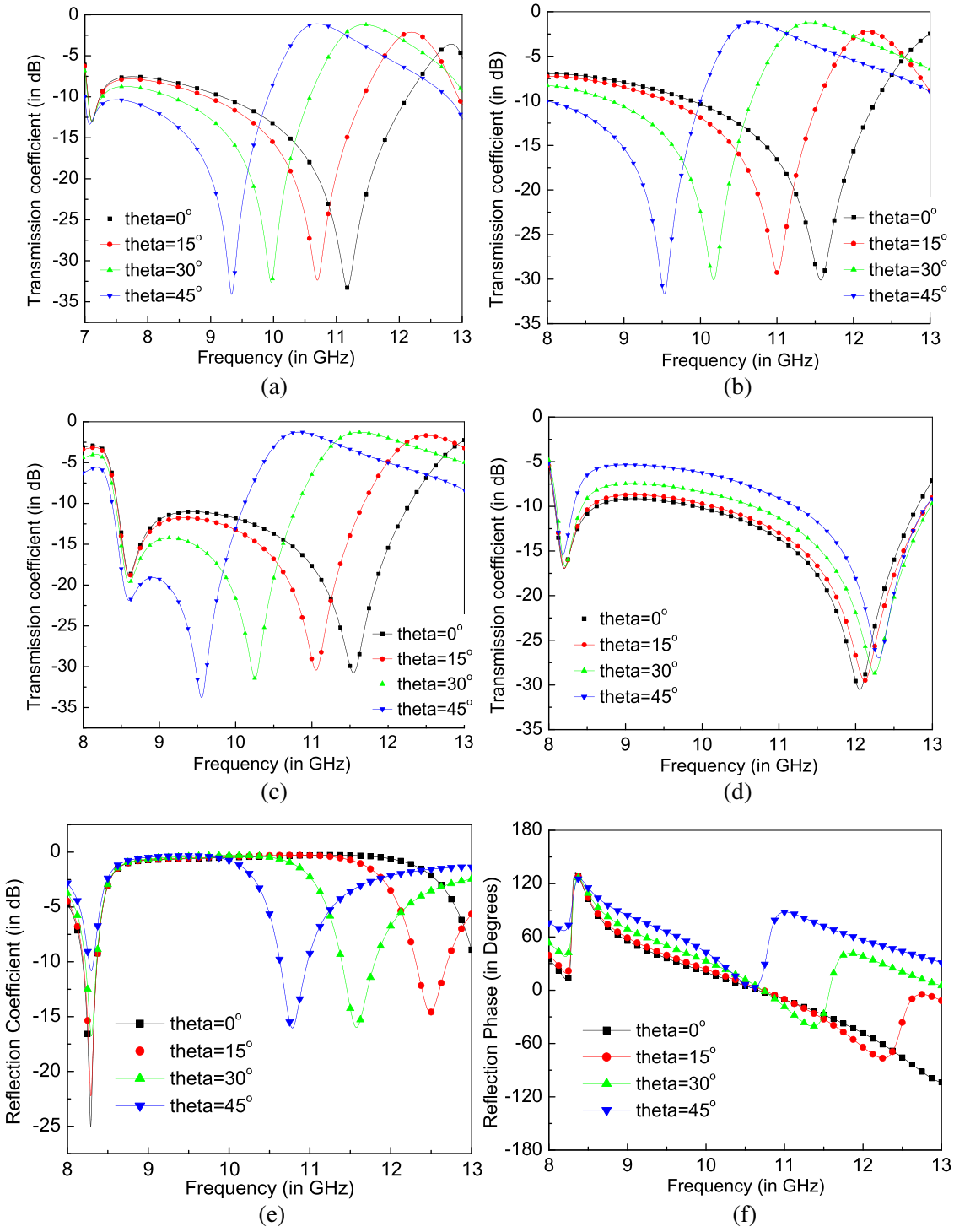

Figure 3. Transmission coefficient characteristics under oblique incidence for (a) structure 1, (b) structure 2 for TE polarization, Transmission coefficient characteristics for the proposed structure for (c) TE and (d) TM polarization respectively for oblique incidence, (e) reflection coefficient characteristics and (f) reflection phase characteristics for oblique incidence for the proposed structure for TE polarization.

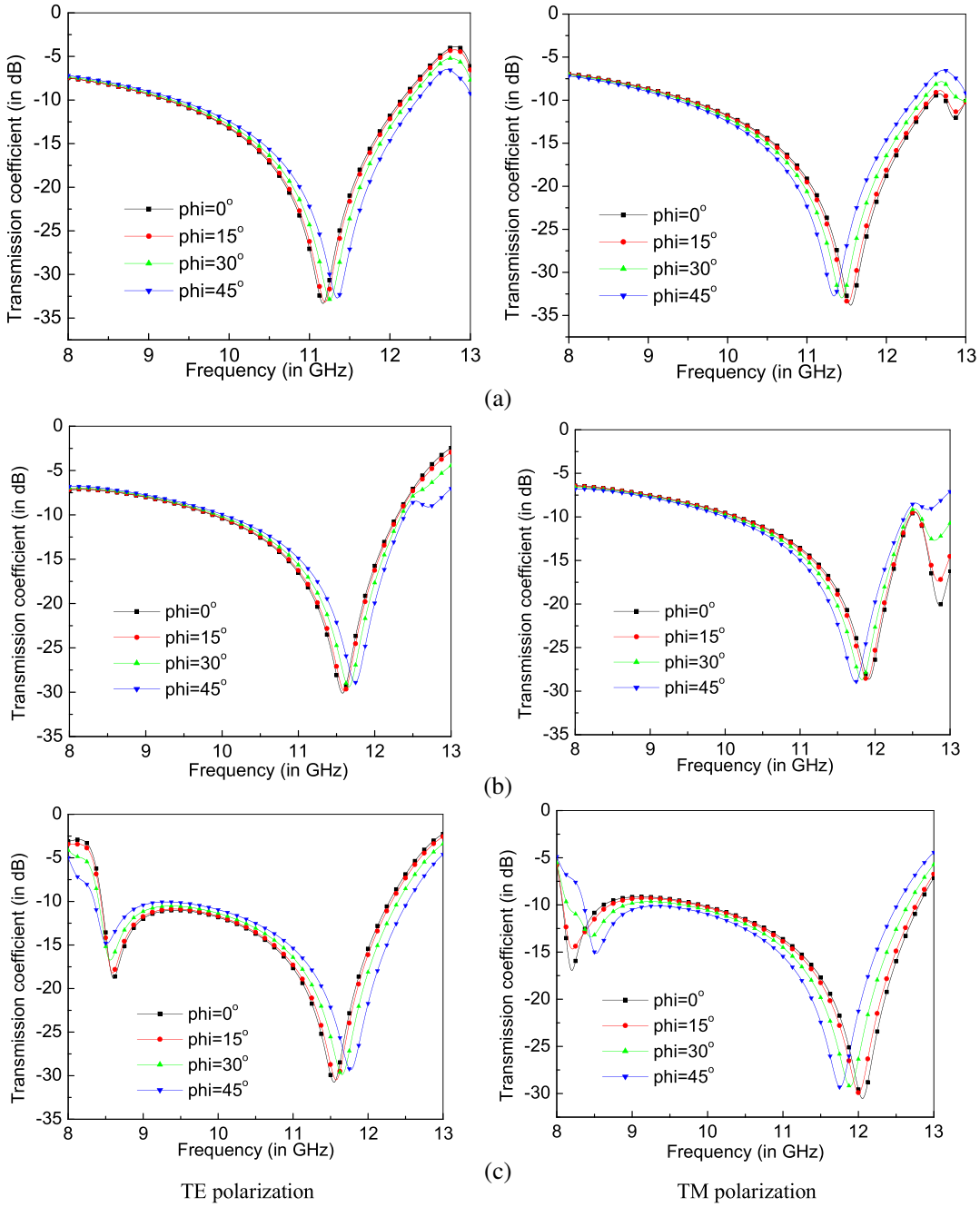

Figure 4. Transmission coefficient characteristics under different polarization angles for TE and TM polarizations for (a) structure 1, (b) structure 2, and (c) proposed FSS.

where Y_{FSS1} and Y_{FSS2} are the admittance of the top and bottom metallic FSS layers respectively and are expressed as $Y_{\mathrm{FSS}i} = \frac{\omega C_i}{1-\omega^2 C_i L_i}$ $(i = 1, 2)$. φ is given as $\varphi = \frac{2\Pi f t_{sub}}{c} \cdot \sqrt{\varepsilon_r - \sin^2\theta}$, and Z_1 for both TE and TM polarizations is given as,

$$Z_1 = \begin{cases} \dfrac{Z_0}{\sqrt{\varepsilon_r - \sin^2\theta}} & \text{for TE polarization [12]} \\ \dfrac{Z_0\sqrt{\varepsilon_r - \sin^2\theta}}{\varepsilon_r} & \text{for TM polarization [12]} \end{cases} \tag{2}$$

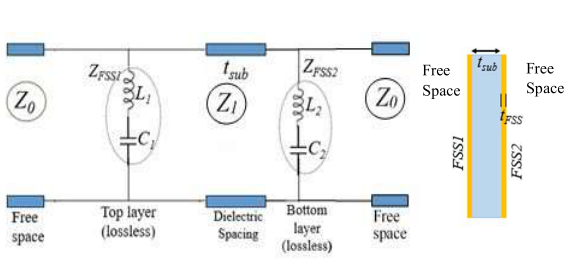

(a)

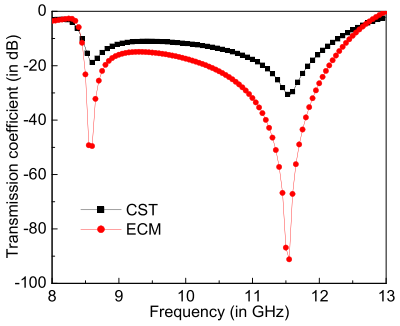

(b)

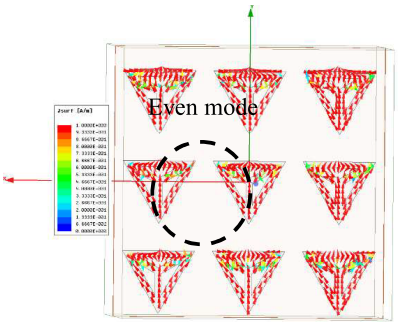

(c)

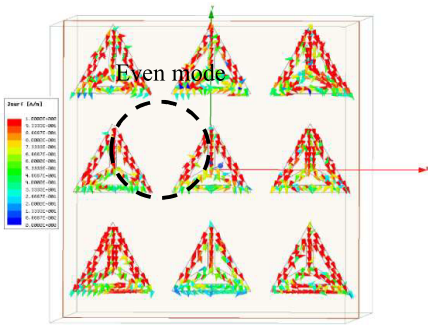

(d)

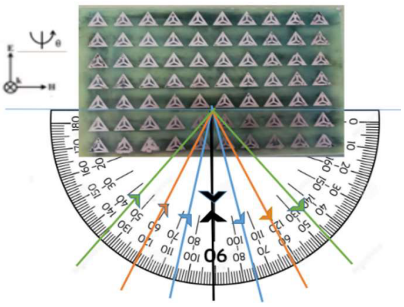

(e)

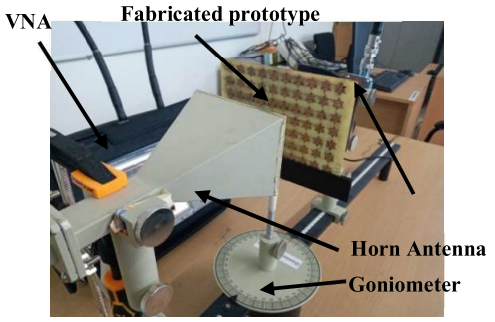

(f)

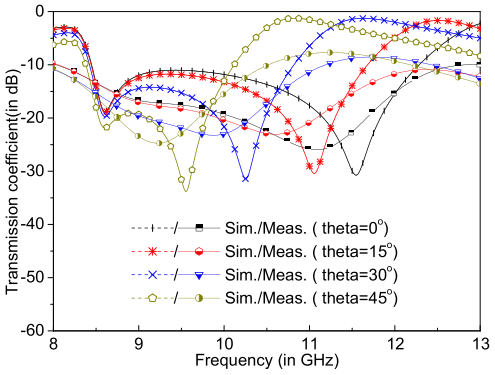

(g)

Angle (Degree)	Structure 1	Structure 2	Structure 3 (Proposed)	Prototype Structure 3
Transmission bandwidth (S_{21}≤-10 dB) (TE Polarization)	Simulated (in GHz)			Measured (In GHz)
0°	9.3-12	10-12.3	8.45-12.28	8.04-12.83
15°	9-11.4	9.7-11.5	8.44-11.68	8.06-12.53
30°	8.5-10.5	8.8-10.6	8.42-10.82	7.8-11.18
45°	7.5-9.8	8.2-10	8.37-10.1	7.86-10.51

(h)

Figure 5. (a) Transmission line equivalent model, (b) comparison between circuit simulation and EM solver results, surface current distribution of (c) bottom and (d) top layers of the proposed FSS structure, (e) fabricated prototype and (f) measurement set up, (g) simulated and measured transmission coefficient characteristics, and (h) simulated and measured transmission bands at different incidence angles.

where $Z_0 = 377\,\Omega$, which is the free-space impedance, f is the frequency, ω the angular frequency, c the speed of light in free space, and θ the angle of incidence. The transmission coefficient (S_{21}) can be represented in terms of $ABCD$ parameters [11] as,

$$S_{21} = \frac{2Z_0}{AZ_0 + B + CZ_0^2 + DZ_0} \tag{3}$$

Here the calculation has been done for TE polarization under normal incidence (i.e., $\theta = 0°$). The frequencies corresponding to transmission coefficient minima (transmission zeros) can be represented by f_{Zi} and given as,

$$f_{Zi} = \frac{1}{2\pi\sqrt{L_i C_i}} \tag{4}$$

Based on Equations (1)–(4), the values of lumped inductors and lumped capacitors are calculated. The inductance and capacitance values obtained are $L_1 = 13.47\,\text{nH}$, $C_1 = 0.0256\,\text{pF}$, $L_2 = 25.44\,\text{nH}$, and $C_2 = 0.0075\,\text{pF}$.

The comparison between the results obtained using CST [15] and ECM is shown in Fig. 5(b). There is a good agreement between the results in terms of the cutoff frequencies and the frequencies corresponding to S_{21} minima. The deviation in S_{21} characteristics is due to the coupling effects between two FSS layers [12] which is not considered in the ECM.

The current distributions of both the bottom and top layers of the FSS structure are shown in Figs. 5(c) and (d), respectively. The surface current distributions between the two sides of adjacent triangular elements are same in direction which shows the even mode coupling [19]. The structural asymmetry of the unit cell geometry in a plane leads to the frequency hopping scattering parameter characteristics under TE polarization as it changes the inductance and capacitance values due to varying angle of incidence.

4. MEASURED RESULTS

A prototype of the proposed RFSS geometry of dimension $150\,\text{mm} \times 98\,\text{mm}$ containing 10×7 unit cell elements has been fabricated using the 'thermal toner transfer method', as shown in Fig. 5(e). The measurement setup for the S parameter characteristics under normal and oblique incidence consists a Vector Network Analyzer (VNA) [Make: Anritsu, Model no: MS2028C], turn table, and X band pyramidal horn antennas, as shown in Fig. 5(f). The measured transmission coefficient characteristics [as shown in Fig. 5(g)] are slightly deviated from the simulated one due to fabrication tolerance, alignment issue, and background noise in free space measurement. However, the frequency shift is clearly visible under TE polarization for different incidence angles, as tabulated in Fig. 5(h).

5. CONCLUSION

The TL element and 3L element have been investigated to design a wideband RFSS unit cell. The proposed single substrate two sided RFSS geometry offers better stopband performance than single layer geometries. The proposed structure provides stopband over the complete X-band for both TE and TM polarizations under normal incidence. For all the two layered models, the stopband frequencies can be reconfigured by varying the angle of incidence of the incident plane wave under TE polarization over the X band. The angle of incidence can be changed manually or automatically with the help of a stepper motor along with a microcontroller interface. The proposed geometry is polarization insensitive under both TE and TM polarizations. Table 1 provides the comparison with some existing works (including both electronically and mechanically tunable structures). The proposed work presents a simple, low cost RFSS solution with better bandwidth which can be used as a reconfigurable reflector for various applications like intelligent walls/RIS based multiplexing system in wireless communication systems [20].

ACKNOWLEDGMENT

The authors are thankful to Mr. Kishore Kumar Das for providing support during fabrication process and measurement of the proposed structure. The first author acknowledges the financial support received from UGC India through a fellowship (NTA Ref. No.: 200510980526 dated10/12/2020).

REFERENCES

1. Munk, B. A., *Frequency Selective Surfaces — Theory and Design*, John Wiley & Sons, New York, 2000.
2. Abadi, S. M. A. M. H., J. H. Booske, and N. Behdad, "Exploiting mechanical flexure as a means of tuning the responses of large-scale periodic structures," *IEEE Trans. Antennas Propag.*, Vol. 64, No. 3, 933–943, Mar. 2016.
3. Ferreira, D., I. Cuiñas, R. F. S. Caldeirinha, and T. R. Fernandes, "3-D mechanically tunable square slot FSS," *IEEE Trans. Antennas Propag.*, Vol. 61, No. 1, 242–250, Jan. 2017.
4. Azemi, S. N., K. Ghorbani, and W. S. T. Rowe, "A reconfigurable FSS using a spring resonator element," *IEEE Antennas Wirel. Propag. Lett.*, Vol. 12, 781–784, Jun. 2013.
5. Silva, A. N., R. G. G. Carvalho, A. G. D. D'Assunção, and J. P. Silva, "Simple and efficient design of reconfigurable FSS with triangular patch elements," *International Applied Computational Electromagnetics Society Symposium — Italy (ACES)*, May 2017.
6. Bai, H., M. Yan, W. Li, J. Wang, L. Zheng, H. Wang, and S. Qu, "Tunable frequency selective surface with angular stability," *IEEE Antennas Wirel. Propag. Lett.*, Vol. 20, No. 6, 1108–1112, Jun. 2021.
7. Guo, M., Y. Zheng, Q. Chen, L. Ding, D. Sang, F. Yuan, T. Guo, and Y. Fu, "Analysis and design of a high-transmittance performance for varactor-tunable frequency-selective surface," *IEEE Trans. Antennas Propag.*, Vol. 69, No. 8, 4623–4632, Aug. 2021.
8. Tian, T., X. Huang, K. Cheng, Y. Liang, S. Hu, L. Yao, D. Guan, Y. Xu, and P. Liu, "Flexible and reconfigurable frequency selective surface with wide angular stability fabricated with additive manufacturing procedure," *IEEE Antennas Wirel. Propag. Lett.*, Vol. 19, No. 12, 2428–2432, Dec. 2020.
9. Abirami, S. B., E. F. Sundarsingh, and V. S. Ramalingam, "Mechanically reconfigurable frequency selective surface for RF shielding in indoor wireless environment," *IEEE Trans. Electromag. Compatibility*, Vol. 62, No. 6, 2643–2646, Dec. 2020.
10. Phon, R., S. Ghosh, and S. Lim, "Active frequency selective surface to switch between absorption and transmission band with additional frequency tuning capability," *IEEE Trans. Antennas Propag.*, Vol. 67, No. 9, 6059–6067, Sept. 2019.
11. Pozar, D. M., *Microwave Engineering*, 3rd Edition, John Wiley & Sons, New York, 2004.
12. Liu, N., X. Sheng, C. Zhang, J. Fan, and D. Guo, "A design method for synthesizing wideband band-stop FSS via its equivalent circuit model," *IEEE Antennas Wirel. Propag. Lett.*, Vol. 16, 2721–2725, Aug. 2017.
13. Chen, Q., S. Yang, J. Bai, and Y. Fu, "Design of absorptive/transmissive frequency-selective surface based on parallel resonance," *IEEE Trans. Antennas Propag.*, Vol. 65, No. 9, 4897–4902, Sept. 2017.
14. Huang, H. and Z. Shen, "Absorptive frequency-selective transmission structure with square-loop hybrid resonator," *IEEE Antennas Wirel. Propag. Lett.*, Vol. 16, 3212–3215, Nov. 2017.
15. Computer Simulation Technology (CST), Version: 2019.
16. Bhattacharya, A., B. Dasgupta, and R. Jyoti, "Design and analysis of ultrathin X-band frequency selective surface structure for gain enhancement of hybrid antenna," *Int. J. RF Microw. Computer-Aided Engg.*, Vol. 31, No. 2, 1–12, Dec. 2020.
17. Parui, S. and A. Chatterjee, "A dual-layer frequency selective surface reflector for wideband applications," *Radioengineering*, Vol. 25, 67–72, Apr. 2016.
18. Kesavan, A., R. Karimian, and A. T. Denidni, "A novel wideband frequency selective surface for millimeter-wave applications," *IEEE Antennas Wirel. Propag. Lett.*, Vol. 15, 1711–1714, Jan. 2016.

19. Ghosh, S. and K. V. Srivastava, "An equivalent circuit model of FSS based matematerial absorber using coupled line theory," *IEEE Antennas Wirel. Propag. Lett.*, Vol. 14, 511–514, Nov. 2014.
20. Zhang, L., M. Z. Chen, W. Tang, J. Y. Dai, L. Miao, X. Y. Zhou, S. Jin, Q. Cheng, and T. J. Cui, "A wireless communication scheme based on space- and frequency-division multiplexing using digital metasurfaces," *Nature Electro.*, Vol. 4, 218–227, Mar. 2021.